Front. Earth Sci. 2019, 13(1): 191–208
https://doi.org/10.1007/s11707-018-0694-z

RESEARCH ARTICLE

Geological significance of the former Xiong'er Volcanic Belt on the southwestern margin of the North China Craton

Guanxu CHEN, Jinhai LUO (✉), Huan XU, Jia YOU, Yifei LI, Zichen CHE

State Key Laboratory of Continental Dynamics (Northwest University), Department of Geology, Northwest University, Xi'an 710069, China

Abstract The rock association of low-grade metasedimentary rocks and greenschists located within the Meso-Cenozoic Liupanshan Fault system on the southwestern margin of the North China Craton (NCC) is regarded as part of the Paleoproterozoic Xiong'er Group. These low-grade rocks are separated by normal faults, with the greenschist located in the hanging walls. Zircon LA–ICP–MS U–Pb ages of the greenschists range from 2455 to 423 Ma, suggesting that they are not Paleoproterozoic in age. The protolith ages (206–194 Ma) of the greenschists were determined by LA–ICP–MS U–Pb dating of zircons from two siltstone interlayers. The petrology and geochemistry of the greenschists reveal that their protolith was continental tholeiitic basalt that formed in an extensional environment such as a continental rift. Thus, it is proposed that the protolith of the greenschists was a mafic volcanic rock of Late Triassic–Early Jurassic age and was metamorphosed during the Jurassic due to tectonism within the Liupanshan tectonic belt. These results show that the greenschists should be reclassified and removed from the Xiong'er Group, and explains why they differ so much from those of typical Xiong'er Group successions in other areas. The formation of the mafic volcanic rocks under conditions of continental rifting differs from that of coeval granitic rocks in the western Qinling Orogen, where the extension occurred during a post-collisional stage in the Late Triassic, which further suggests that the southwestern margin of the NCC became an extensional setting after the Late Triassic.

Keywords southwestern margin of the NCC, Paleoproterozoic Xiong'er Group, greenschist, detrital zircon U–Pb geochronology, Late Triassic to Early Jurassic

1 Introduction

The Paleoproterozoic Xiong'er Group, which crops out at the southern margin of the North China Craton (NCC), consists mainly of a thick succession of volcanic rocks, reflecting the intense tectono-magmatic events that occurred after cratonization of the NCC basement (Zhao et al., 2007). However, previous studies of the Xiong'er Group have largely been confined to the Xiaoqinling-Xiong'ershan Region in the southern margin of the NCC. A succession of low-grade metamorphic rocks exposed in Fengjiashan along the southwestern margin of NCC has been classified as the Paleoproterozoic Xiong'er Group on the basis of stratigraphic correlations (Fig. 1; Bureau of Geology and Mineral Resources of Shaanxi Province, 1989), and is the westernmost occurrence yet discovered. The lower boundary of these rocks is not exposed as they are overlain by Mesoproterozoic Gaoshanhe Group platform carbonates, separated by a fault. This study investigates the nature of these westernmost outcrops of the Xiong'er Group which is comprised of two major rock types: 1) low-grade metasedimentary rocks, including gray–green, gray–red sericitic quartzschist, thinly bedded calcareous slate, reworked sandstone, and finely laminated limestone; and 2) greenschist-facies rocks, including epidote–actinolite schists and albite–actinolite schists. Zhou et al. (1994) obtained a Sm–Nd model age of 1672±81 Ma for these greenschists and classified them as part of the Xiong'er Group. However, the rock types and ages are markedly different from those of the typical Xiong'er Group exposed in the Xiong'ershan, Xiaoshan, and Xiaoqinling Mountains (Fig. 1(b)), consisting of a thick succession of volcanic rocks, ranging from basaltic andesite, andesite, and dacite to rhyolite with an age of 1.85–1.70 Ga (Lu et al., 2002), 1.80–1.75 Ga (Zhao et al., 2002, 2004, 2007), 1.84–1.77 Ga (Hou et al., 2008), 1.78 Ga (Peng et al., 2008, 2015), 1.78–1.75 Ga (He et al., 2009; Zhao et al., 2009), 1.76 Ga (Wang et al., 2010), 1800–1770 Ma (Cui et al., 2011), 1.80–1.45 Ga (Deng et

Received August 3, 2017; accepted November 23, 2017

E-mail: luojh@nwu.edu.cn

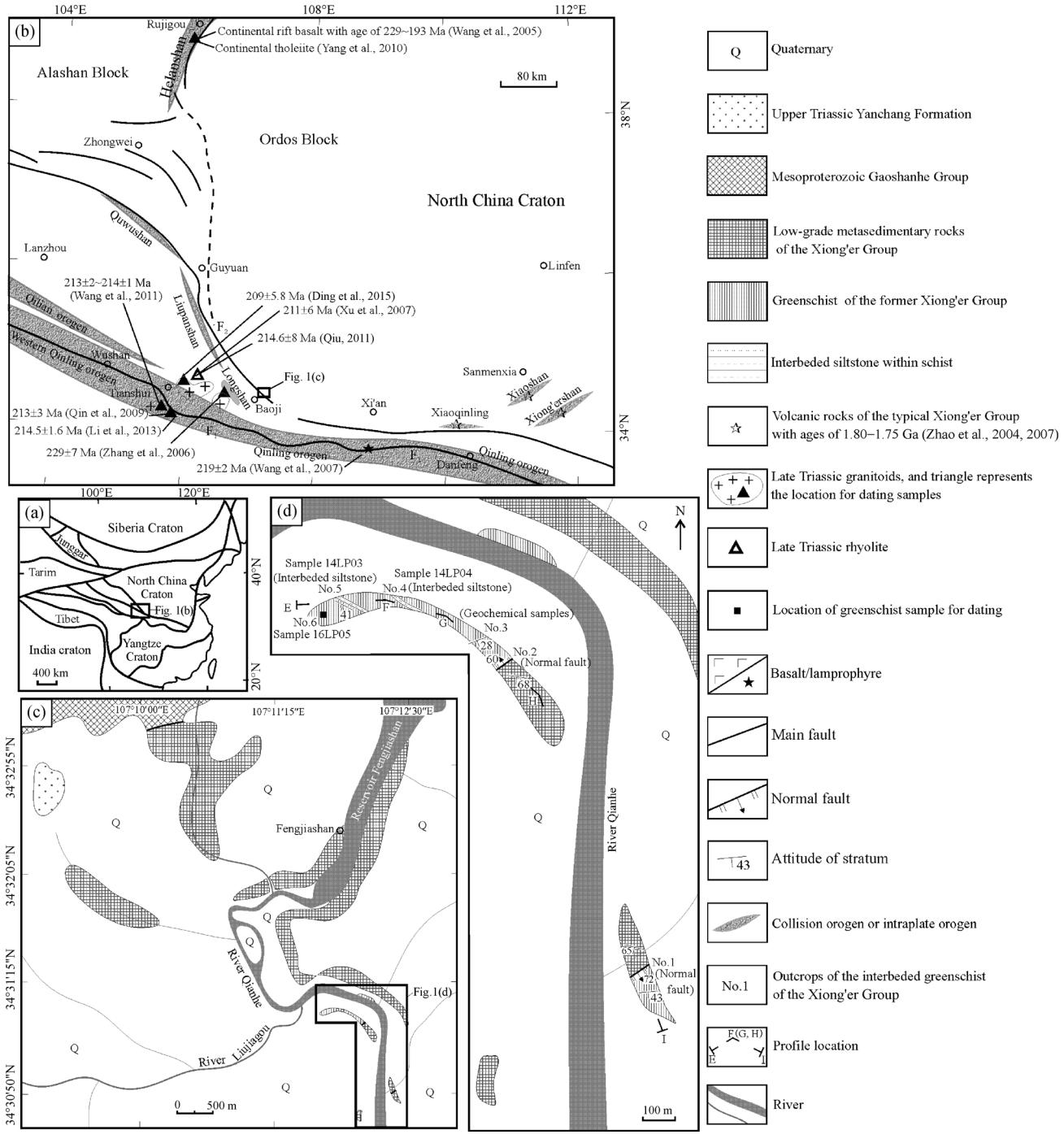

Fig. 1 Geological map around the former Xiong'er Group in the southwestern margin of the North China Craton (modified from the 1:200,000 Baoji Geological Map (1966), 1:250,000 Baojishi Geological Map (2003), and this paper). (a) Tectonic map of China, showing the location of the study area; (b) geological map of the study area; (c) geological map of the Xiong'er Group; (d) enlarged geological map of greenschists in the Xiong'er Group. F_1-Shangdan suture, F_2-Liupanshan fault system.

al., 2013), ~1.80–1.78 Ga (Zhai et al., 2015) and 1.80–1.00 Ga (Zhang et al., 2015). Field mapping of the Xiong'er Group in the study area has revealed that the greenschists and low-grade metasedimentary rocks are separated by normal faults, the greenschists occur in the hanging walls of the faults (Fig. 1(d); localities No. 1 and No. 2), and two siltstone layers are interbedded with the greenschists (Fig. 2). In this study, we focus on the volcanic rocks that are proposed to be part of the Xiong'er Group. To determine the environment of formation and age of the protolith of the greenschists, their geochemical characteristics were analyzed, and LA–ICP–MS zircon U–Pb ages

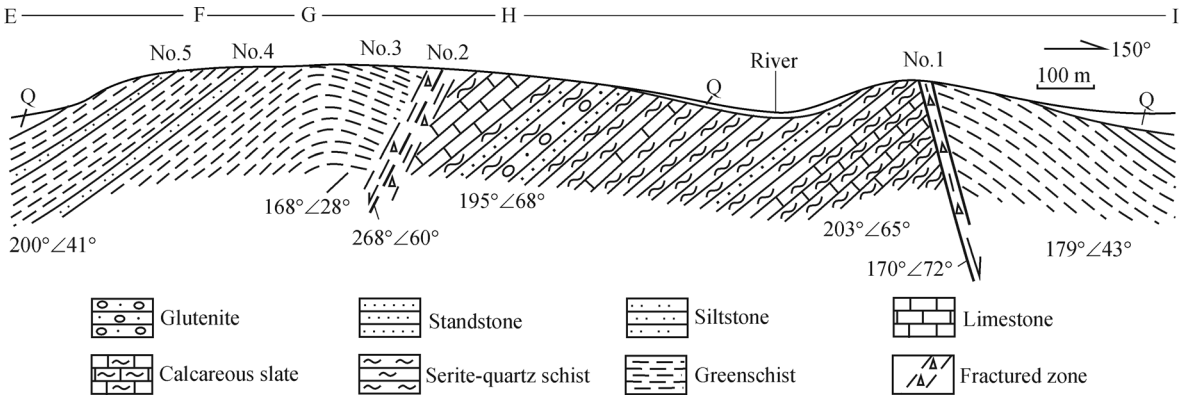

Fig. 2 Cross-section of the Xiong'er Group in the study area. The location of the cross-section is shown in Fig. 1(d).

were obtained for the greenschists and interbedded siltstones. Our results suggest that the greenschists do not belong to the Paleoproterozoic Xiong'er Group, and that the protoliths of the greenschists indicate continental rifting during the Late Triassic to Early Jurassic.

2 Petrological features of the greenschists

The greenschists and low-grade metasedimentary rocks in the study area are exposed in the banks of the Qianhe River (localities No. 1 and No. 2; Figs. 1(c), 1(d), and 2). The contacts between these two lithological units are normal faults, and the greenschists formed in the hanging walls (Figs. 3(a)–3(c)). Fault breccias are weakly cemented, indicating that they formed in a near-surface, low-temperature structural setting (Figs. 3(a) and 3(c)). The greenschists are overlain by Quaternary loess.

The greenschists are green in color, show weak deformation, and contain quartz veins that are concordant with schistosity in the greenschists, which formed during greenschist-facies metamorphism. The orientation of schistosity in the greenschists varies from 168°∠28° to 179°∠43°, and 200°∠41° (Fig. 2). The greenschists contain chlorite, epidote, albite, and actinolite; the chlorite and albite show fibroblastic and lepidoblastic textures (Fig. 4). This mineral assemblage, together with the occurrence of interbedded siltstones, suggests that the protolith of the greenschist was an intermediate–basic volcanic rock.

The interbedded siltstones, which are exposed at localities No. 4 and No. 5 (Figs. 1(d) and 2), are aqua-colored and have well-developed lamellae oriented parallel to the schistosity. The siltstones consist of three to five thin lamellae that are each 7–10 cm thick (Figs. 3(e) and 3(f)).

3 Analytical methods and results

3.1 Analytical methods

Major and trace element analyses were conducted at the State Key Laboratory of Continental Dynamics, Northwest University, Xi'an, China. The samples were washed and crushed in a jaw crusher to 60 mesh. Sixty grams of the sample were then milled in a WC Mill (T1-100, CMT) to 75 μm for whole-rock analysis. Major element oxides were measured using a Rigaku RIX 2100 XRF with Li-borate glass disks. Trace and rare earth elements were measured using an Agilent 7500a ICP–MS. Samples (50 mg) were dissolved in a sealed high-temperature and high-pressure bomb using equal parts of HF and HNO_3. International rock standards BHVO-1 and AGV-1 (from USGS) were used to calibrate major and trace element analyses, to ensure that precision and accuracy were within 5%.

Detrital zircons were analyzed by LA–ICP–MS. The zircons were extracted from the siltstones using heavy liquid and magnetic separation, hand-picked under a binocular microscope, mounted in epoxy resin, and polished until the grain centers were exposed. Cathodoluminescence (CL) imaging was done using a Quanta 400FEG environmental scanning electron microscope, equipped with an Oxford energy dispersive spectroscopy system and a Gatan CL3 + detector. The U–Pb analyses were conducted on an Agilent 7500a ICP–MS instrument equipped with a 193 nm ArF-excimer laser, and a homogenizing, imaging optical system. A fixed spot size of 30 μm and a laser repetition rate of 6 Hz were applied for all analyses, and helium was used as the carrier gas. The standard silicate glass NIST 610 was used to optimize the instrument and obtain maximum signal intensity (^{238}U signal intensity > 460 cps/($\mu g \cdot g^{-1}$)) and low oxide production (ThO/Th $< 1\%$). The U/Th ion-signal intensity ratio was measured to monitor complete zircon vaporization (Günther and Hattendorf, 2005). A single spot was measured in each zircon. The ICP–MS measurements were conducted using time-resolved analysis operating in fast peak jumping mode of 20 ms per peak, and in DUAL detector mode using a short integration time. $^{207}Pb/^{206}Pb$, $^{206}Pb/^{238}U$, $^{207}Pb/^{235}U$, and $^{208}Pb/^{232}Th$ values were calculated using GLITTER 4.0 (Macquarie University). The ratios were corrected using Harvard zircon 91500 as an external standard, with a recommended $^{206}Pb/^{238}U$ age of

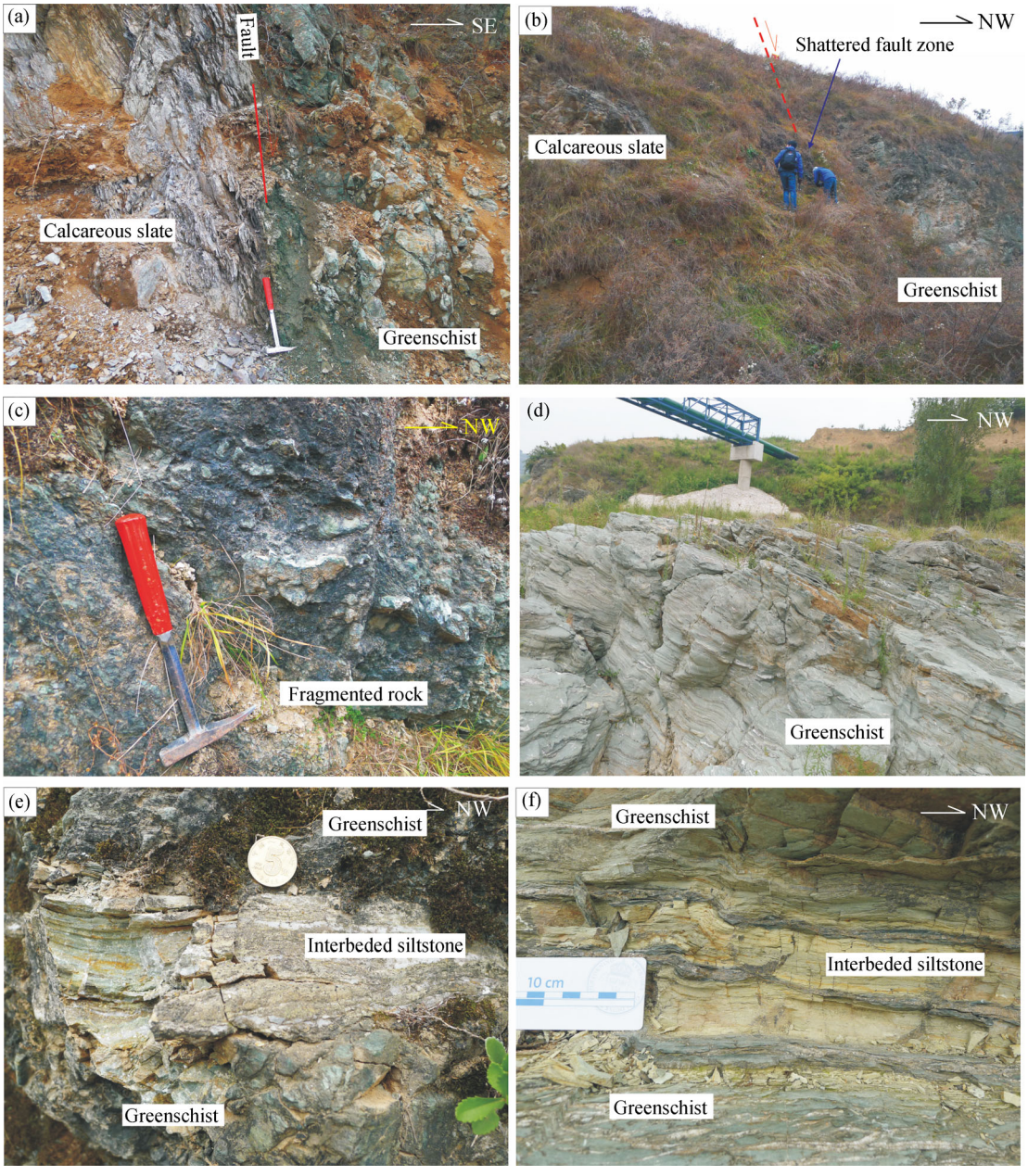

Fig. 3 Outcrop photographs of greenschists in Fengjiashan. (a) Normal fault between greenschist and calcareous slate at outcrop No. 1; (b) contact relationships between greenschists and calcareous slates at outcrop No. 2; (c) enlarged photograph of the brecciated fault zone at outcrop No. 2; (d) greenschists at outcrop No. 3, where samples for geochemical analysis were collected; (e)–(f) interbedded siltstone and greenschist at outcrops Nos. 4 and 5. Locations of outcrops Nos. 1–5 are shown in Fig. 1(d) and Fig. 2.

1065.4±0.6 Ma (Wiedenbeck et al., 1995, 2004), to correct for both instrumental mass bias and depth-dependent elemental and isotopic fractionation. Concordia diagrams and weighted mean calculations were plotted using Isoplot (v. 2.49; Ludwig, 2001). Uranium, Th, and Pb concentrations were calibrated using ^{29}Si as an internal standard and NIST SRM610 as an external standard. Zircon standards 91500 and GJ-1 were analyzed as unknowns.

3.2 Results

3.2.1 Major and trace elements in the greenschists

The major and trace element abundances of greenschists from the Xiong'er Group are listed in Table 1. The loss on ignition (LOI) of the samples ranges from 3.1% to 11.0% (average LOI = 4.9%), suggesting that the samples are

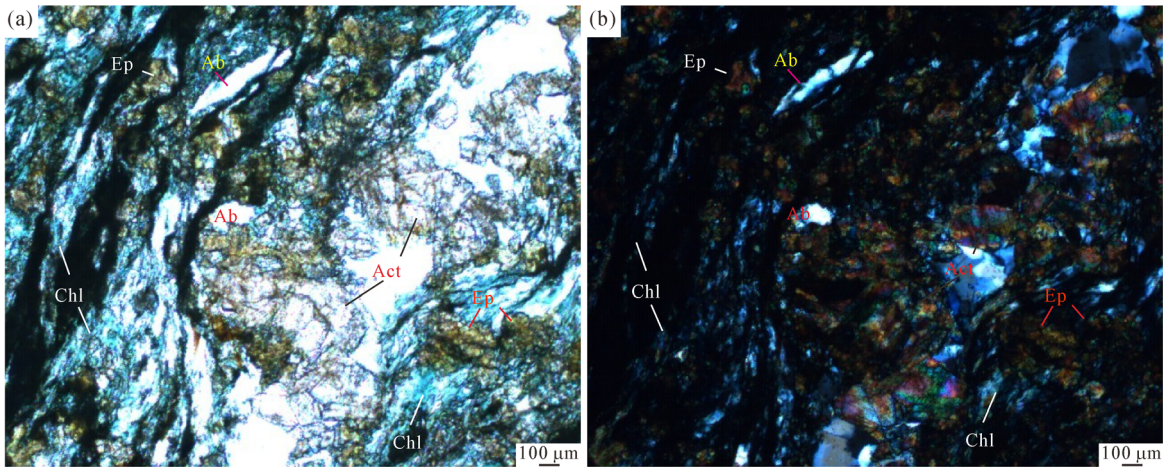

Fig. 4 Microphotographs of the greenschists. (a) Plane-polarized light; (b) cross-polarized light. Ab-albite, Act-actinolite, Chl-chlorite, Ep-epidote.

highly altered and consistent with the greenschist facies metamorphism of the samples which have been taken into consideration where major elements have been used in calculations. Silica values of the greenschists are low (46.2%–51.7%; average SiO_2 = 48.7%), indicating they are basic. Titanium contents range from 1.4% to 2.1% (average TiO_2 = 1.9%), higher than values of oceanic tholeiites (1.4%) and island arc tholeiites (0.8%), and lower than oceanic island basalts (OIB, 2.2%; Pearce, 1982). Total alkali (ALK = $K_2O + Na_2O$) contents range from 1.3% to 3.3% (average ALK = 2.6%), and $Na_2O > K_2O$. The samples are classified as basalt in the TAS diagram for volcanic rocks (Fig. 5), and thus it is likely that the protolith of the greenschist was basaltic. In addition, Mg# = 34.1–44.7 (average Mg# = 40.8), which is lower than that of primitive basaltic magma (68–75; Frey et al., 1978), suggesting that the basaltic protolith was formed from the fractionation of a primitive basaltic magma.

Total REE (ΣREE) range from 46.45 to 69.20 ppm (parts per million) (average ΣREE = 64.95 ppm), and LREE are slightly enriched relative to HREE [$(La/Yb)_N$ = 1.34–1.59]. The chondrite-normalized REE trends of the greenschists are similar to that of E-MORB (Fig. 6(a)), and they have no Eu anomalies (δEu = 0.94–1.04). The variability shown in REE trends (Fig. 6(b)) suggests that the basaltic protolith was subjected to crustal contamination. Large-ion lithophile (LILE) and high-field-strength elements (HFSE) are relatively enriched, but Nb, Ta, and P are relatively depleted. The geochemical characteristics of the greenschists are consistent with those of continental tholeiite. Greenschist samples fall into the sub-alkaline field in the SiO_2–ALK diagram and into the tholeiite field in an AFM diagram, which indicates that the protolith of the greenschists was a sub-alkaline tholeiitic basalt (Figs. 7(a) and 7(b)). Samples fall into the "intracontinental rift and continental marginal rift tholeiite" field in log–log Th/Hf–Ta/Hf and La/Zr–Nb/Zr discrimination diagrams, which suggests that the greenschist protolith was tholeiitic and formed in an intracontinental or continental marginal rift (Fig. 8).

3.2.2 Zircon U–Pb geochronology of the greenschists

Zircon LA–ICP–MS U–Pb dating was performed on the greenschist (sample 16LP05) exposed at outcrop No. 6 (Fig. 1(d)). CL images show that the zircons are variable in size and that some have rounded margins (Fig. 9), possibly caused by abrasion or melting. Some zircons have inner cores (e.g., zircon grains of spot analyses 6, 15, and 20 in Fig. 9), and some show clear growth zoning, revealing their complex history. Most zircons are characterized by columnar and euhedral shapes, clear magmatic zoning, and Th/U > 0.1, which all indicate an igneous origin. A small number of zircons have Th/U < 0.1, indicating a possible metamorphic origin.

Thirty-six analyses were conducted on 36 zircon grains from greenschist sample 16LP05, with 21 analyses producing reliable data. The U–Pb data are presented in Table 2 and U–Pb concordia plots are shown in Fig. 10. The concordant or nearly concordant ages range from 2455 to 423 Ma. Given that the youngest zircon age of the greenschist sample is much older than the youngest age obtained from the detrital zircons in the clastic interlayers, the zircon greenschist ages do not represent the formation age of the greenschist protolith. However, it is clear that the many young zircon ages are inconsistent with the rocks that comprise the Xiong'er Group.

3.2.3 U–Pb geochronology of detrital zircons from interbedded siltstones

U–Pb dating was performed on detrital zircons from interbedded siltstones (samples 14LP04 and 14LP03) exposed at outcrops No. 4 and No. 5, respectively (Figs. 1(d) and 2). The zircons are variable in size and some have

Table 1 Major-element (wt%) and trace-element (ppm) compositions of greenschists of the former Xiong'er Group in the southwestern margin of the NCC

Composition	14LP05	14LP06	14LP07	14LP08	14LP09	14LP10	14LP11	14LP12	14LP13	14LP14
SiO_2	46.06	45.00	48.63	44.75	47.71	45.56	44.33	46.52	47.28	46.50
TiO_2	1.28	2.03	1.81	1.58	1.70	1.85	2.02	1.86	1.72	1.77
Al_2O_3	10.18	14.10	13.13	12.38	12.83	13.78	15.57	13.26	13.00	13.89
$^{T}Fe_2O_3$	9.43	15.98	14.85	12.22	14.23	14.50	16.24	15.05	15.07	14.28
MnO	0.15	0.22	0.19	0.17	0.20	0.18	0.19	0.20	0.21	0.20
MgO	3.67	7.01	6.56	4.23	5.58	5.25	4.87	7.04	6.57	6.37
CaO	15.33	9.05	9.35	14.00	10.64	10.52	11.38	9.84	9.88	11.11
Na_2O	2.58	2.61	1.93	2.18	2.59	2.35	1.06	2.12	2.22	2.25
K_2O	0.34	0.23	0.39	0.30	0.32	0.20	0.14	0.38	0.20	0.20
P_2O_5	0.10	0.15	0.14	0.12	0.13	0.14	0.16	0.14	0.13	0.13
LOI	10.95	3.46	3.15	8.29	3.82	5.81	3.84	3.09	3.59	3.05
Total	100.11	99.84	100.13	100.23	99.75	100.14	99.80	99.50	99.87	99.75
$Mg^{\#}$	40.06	43.07	43.24	37.38	40.34	38.44	34.09	44.65	42.92	43.48
Rb	3.72	2.56	4.44	3.90	4.93	2.24	2.25	4.29	2.16	2.08
Ga	13.6	20.3	20.7	17.9	18.6	19.9	24.4	20.9	19.9	21.6
Sr	171	393	408	297	205	206	467	306	348	573
Y	22.7	34.1	30.3	27.0	27.9	30.0	33.8	30.7	27.2	29.4
Zr	72.1	112	102	87.5	94.5	101	111	101	94.4	96.1
Nb	3.70	5.90	5.30	4.55	4.88	5.24	5.78	5.24	4.88	5.02
Cs	0.250	0.075	0.052	0.530	0.430	0.092	0.370	0.055	0.064	0.063
Ba	55.6	65.2	107	82.6	79.2	52.1	67.0	101	52.8	43.0
Hf	1.83	2.91	2.65	2.27	2.44	2.58	2.89	2.62	2.43	2.46
Ta	0.25	0.38	0.35	0.30	0.32	0.35	0.38	0.35	0.32	0.33
Pb	0.81	0.94	1.29	1.27	1.35	1.17	2.16	0.97	1.62	1.90
Th	0.43	0.64	0.58	0.49	0.54	0.61	0.63	0.58	0.53	0.55
U	0.12	0.18	0.18	0.14	0.16	0.17	0.19	0.16	0.15	0.16
La	4.91	6.89	5.96	5.26	5.42	5.77	6.50	6.04	5.32	5.75
Ce	12.5	18.2	16.0	13.8	14.7	15.8	17.4	15.9	14.3	15.1
Pr	1.92	2.88	2.52	2.18	2.30	2.50	2.75	2.53	2.27	2.39
Nd	9.67	14.4	12.6	11.0	11.7	12.6	13.8	12.7	11.4	12.0
Sm	2.92	4.50	4.01	3.48	3.76	4.01	4.36	4.07	3.63	3.85
Eu	0.96	1.52	1.44	1.27	1.30	1.39	1.55	1.49	1.28	1.36
Gd	3.36	5.23	4.66	4.08	4.36	4.70	5.14	4.72	4.25	4.49
Tb	0.60	0.94	0.84	0.73	0.77	0.84	0.92	0.84	0.77	0.81
Dy	3.86	5.97	5.36	4.77	5.01	5.36	5.95	5.41	4.88	5.10
Ho	0.79	1.22	1.11	0.98	1.03	1.10	1.24	1.12	1.01	1.06
Er	2.28	3.46	3.13	2.77	2.86	3.05	3.45	3.16	2.84	2.96
Tm	0.33	0.49	0.45	0.40	0.42	0.44	0.50	0.45	0.40	0.43
Yb	2.08	3.09	2.89	2.62	2.63	2.80	3.25	2.94	2.67	2.82
Lu	0.32	0.46	0.42	0.38	0.39	0.41	0.47	0.43	0.39	0.41
ΣREE	46.45	69.20	61.44	53.82	56.61	60.75	67.30	61.80	55.48	58.51
$(La/Yb)_N$	1.59	1.50	1.39	1.35	1.39	1.39	1.35	1.38	1.34	1.37
δEu	0.94	0.95	1.02	1.03	0.98	0.98	1.00	1.04	1.00	1.00

Note: $Mg^{\#}$ = Mg/(Mg + Fe) ionic amount ratio.

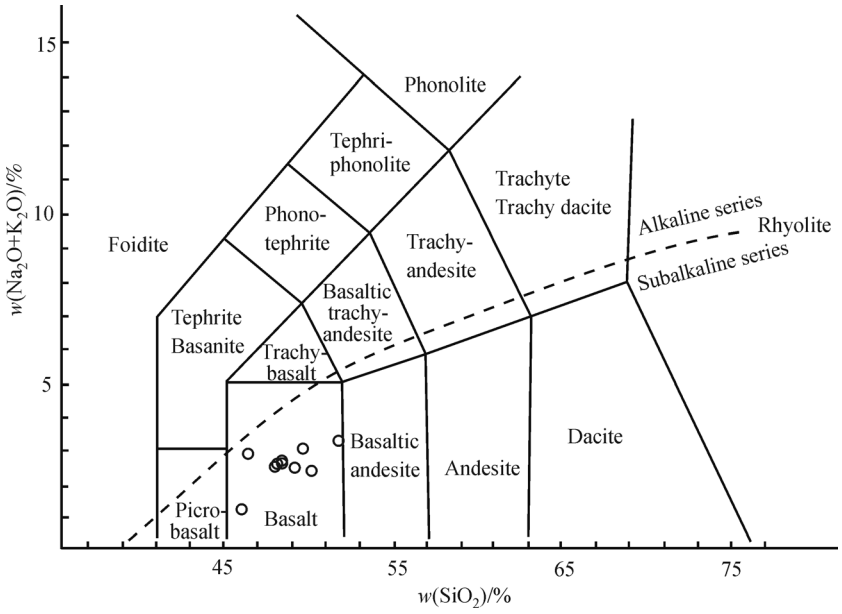

Fig. 5 TAS diagram (after Le Bas et al., 1986) for the greenschists.

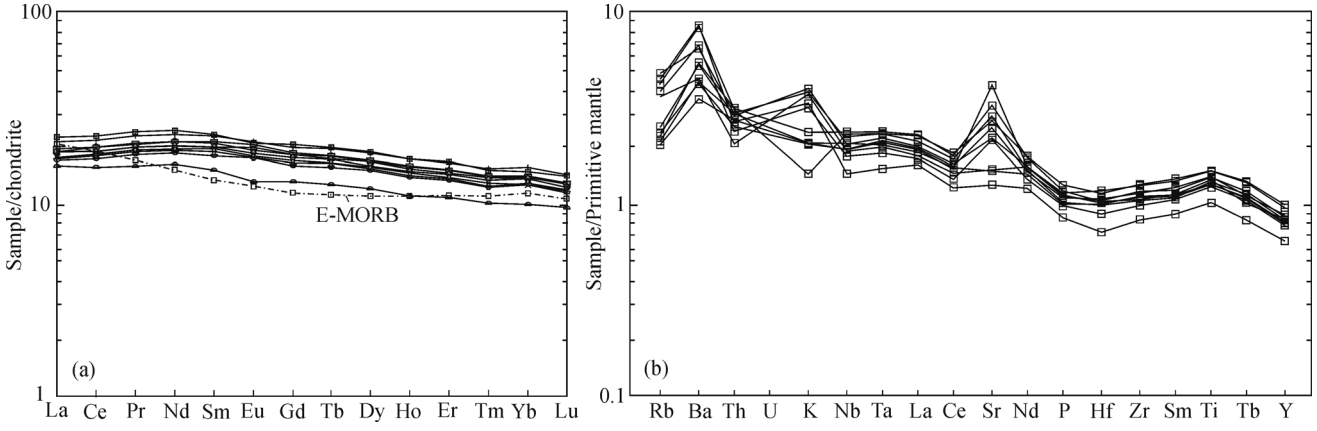

Fig. 6 (a) Chondrite-normalized REE pattern for the greenschists (chondrite data from Boynton, 1984), (b) primitive-mantle-normalized spider diagram for the greenschists of the Xiong'er Group (primitive mantle data from Sun and McDonough, 1989).

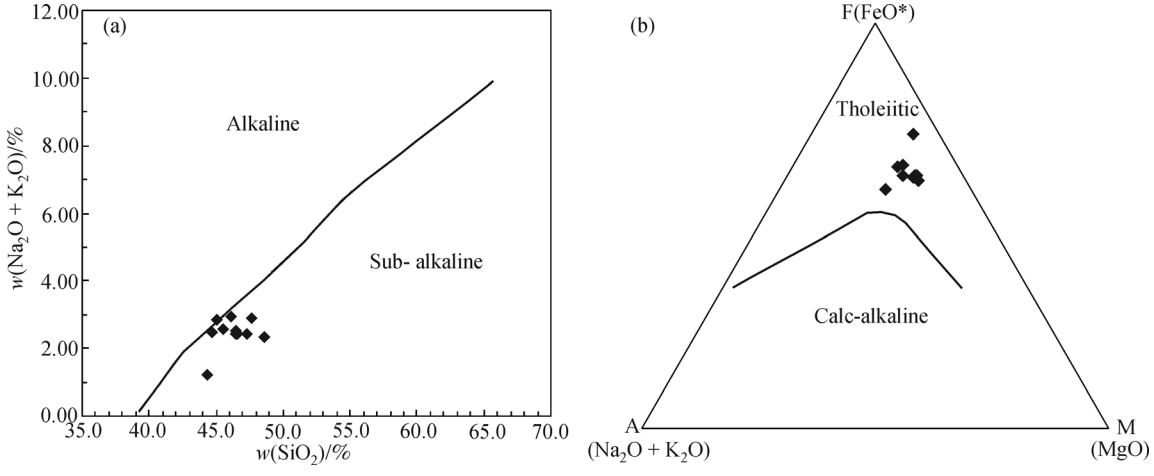

Fig. 7 (a) SiO_2–ALK discrimination diagram (after Irvine and Baragar, 1971) for the greenschists. (b) AFM discrimination diagram for the greenschists.

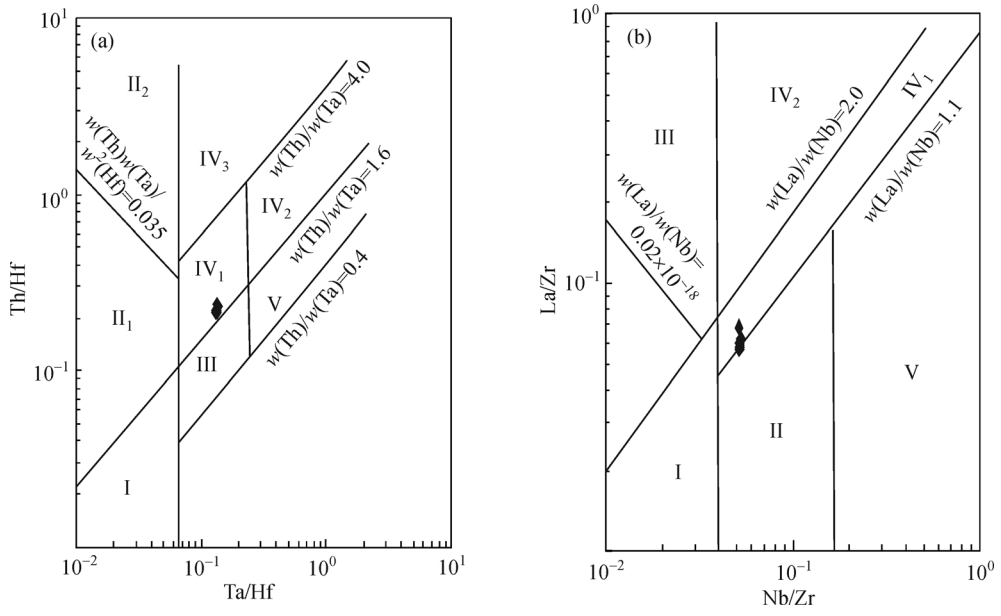

Fig. 8 (a) Log Th/Hf–Ta/Hf and (b) Log La/Zr–Nb/Zr discrimination diagrams for the greenschists. I-divergent margin; II-convergent margin; II_1-oceanic island arc basalt; II_2-continental margin island arc; III-oceanic intraplate oceanic island, seamount basalt area, and T-MORB and E-MORB; IV-continental plate; IV_1-intracontinental rift and continental marginal rift tholeiite; IV_2-intracontinental rift alkaline basalt; IV_3-continental extensional or initial rift basalt; V-mantle plume basalt (after Li et al., 2013).

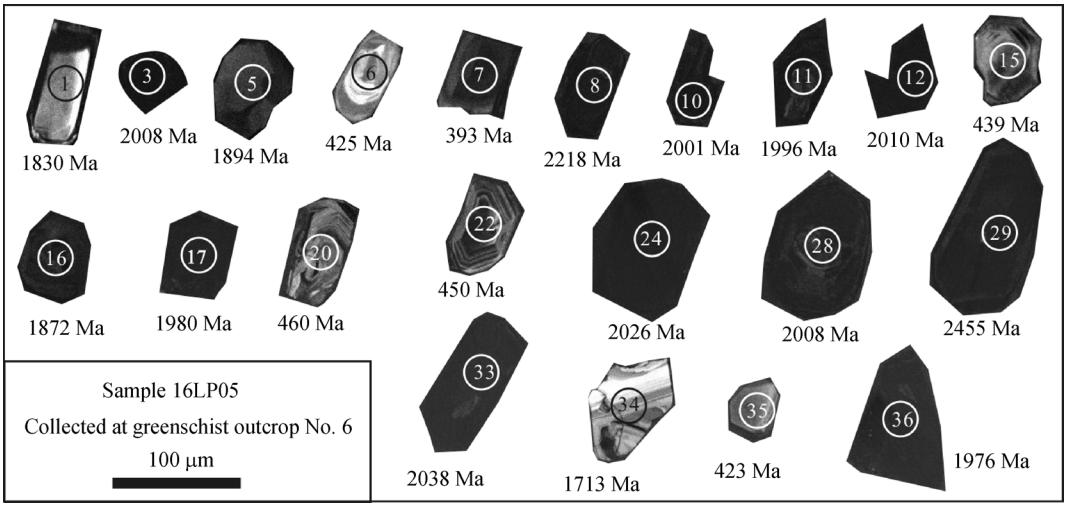

Fig. 9 Cathodoluminescence (CL) images of zircons from the greenschists. Circles indicate analysis sites, and figures within the circles are analysis numbers; the ages are given below the corresponding zircons.

rounded margins (Fig. 11), indicating a detrital origin. However, some are columnar and euhedral, suggesting they have not been transported far from their source. Individual zircon grains (e.g., analyses 13, 19, and 21 in sample 14LP03; Fig. 11) have cores, and some (e.g., analyses 1, 20, 29, 30, 33, and 40 in sample 14LP04; Fig. 11) show clear growth zoning, revealing a complex history. Magmatic zoning is also clear in most CL images, and their Th/U values are greater than 0.1, indicating an igneous origin.

Thirty-four analyses were conducted on 33 zircon grains from sample 14LP03, with 24 yielding reliable ages. Forty analyses were performed on 34 grains from sample 14LP04, 33 of which were retained. The U–Pb data are listed in Table 2 and concordia plots are shown in Fig. 12. The concordant zircons from both siltstone samples yield similar ages: sample 14LP03 yields concordant U–Pb ages ranging from 2462 to 206 Ma, while sample 14LP04 yields concordant U–Pb ages from 3039 to 194 Ma. Both samples show age peaks at 2000 and 400 Ma. The youngest ages

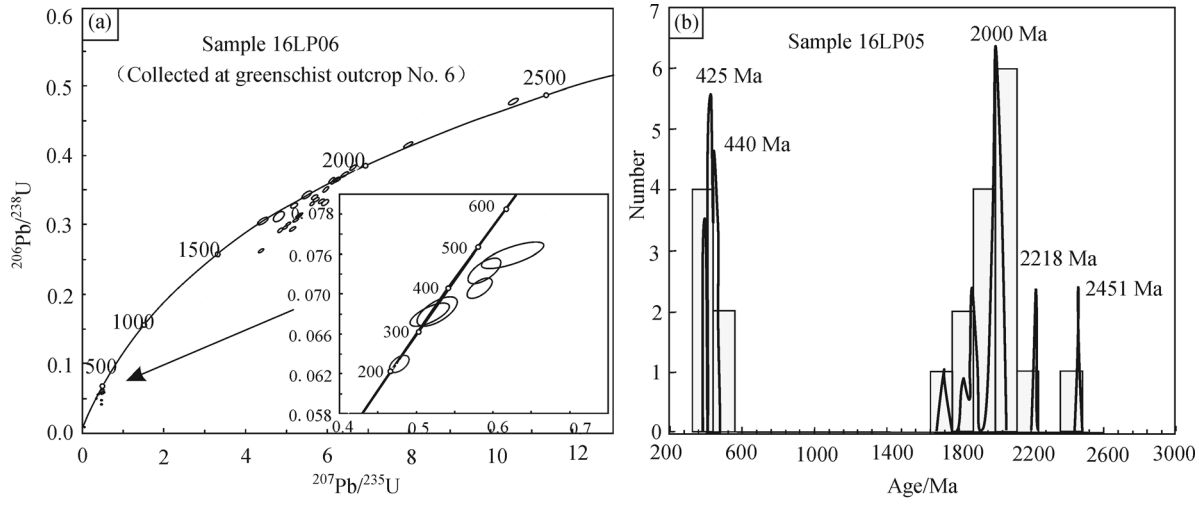

Fig. 10 Concordia diagrams for the greenschist samples. Interpreted ages are $^{206}Pb/^{238}U$ for zircons with ages of < 1.0 Ga and $^{207}Pb/^{206}Pb$ for zircons with ages of > 1.0 Ga.

from both samples are similar (206 and 194 Ma). Sample 14LP04 also yields ages of 222, 228, and 229 Ma, which are close to the youngest. The youngest ages represent the maximum depositional age of the sediments, indicating that the greenschist protolith is younger than the Late Triassic or Early Jurassic.

4 Discussion

4.1 Age of the greenschist protolith

The age of the greenschist protolith cannot be determined using stratigraphic relationships; therefore, the ages of detrital zircons are used to indirectly determine this age. Figures 3(e) and 3(f) show that the siltstones have not been extensively metamorphosed, meaning it is unlikely that the youngest ages from samples 14LP03 (206±3 Ma) and 14LP04 (194±3 Ma) represent the timing of metamorphism. Furthermore, the detrital zircons clearly show internal magmatic zoning, and have magmatic Th/U values (0.55 and 0.45). Thus, these dates represent the ages of the source of the siltstones, indicating that the continental tholeiite protolith of the greenschists could not have been formed earlier than the siltstones (194–206 Ma).

It is proposed that the protolith of the greenschists was formed in the Late Triassic to Early Jurassic based on the following observations.

1) The zircons yielding Late Triassic to Early Jurassic ages are characterized by euhedral crystals and do not display extensive abrasion. This indicates that the source area of the zircons was near the area of sedimentation and that the zircons may have crystallized in the protolith of the greenschists itself.

2) Based on field observations, the protolith could not have formed before 194–206 Ma, nor could it have formed much later, such as in the Cenozoic, as younger clastic rocks of the Lower Cretaceous Liupanshan Group, which are widely distributed along the southwestern margin of the NCC, show no evidence of metamorphism. In the western Qinling Orogen, bimodal volcanism, comprised of kamafugite, carbonatite, shoshonite, and rhyolite, erupted between 23 and 7.1 Ma in an extensional environment (Yu et al., 2011); therefore, the study area and its surrounds likely experienced the same extension. Since the protolith was metamorphosed to conditions of greenschist facies, it must pre-date the bimodal volcanism.

3) The Late Triassic to Early Jurassic extensional setting of the study area favored the formation of the protolith of the greenschists. The sedimentary record preserved on the southwestern margin of the NCC extends into the Late Triassic (Zhao et al., 2006; Deng et al., 2008). Upper Triassic gray–green sandstone and variably colored shale of the Yanchang Formation occured in the study area (Fig. 1(b)). While Late Triassic to Early Jurassic magmatic rocks have not been identified on the southwestern margin of the NCC. A series of Late Triassic granitoids occurred in the western Qinling Orogen, and a lamprophyre of similar age occurred in the central part of the Shangdan Suture (Fig. 1(b); Table 3). These sedimentary and magmatic occurrences indicate that extension in the region occurred during the Late Triassic.

4) No Early Jurassic magmatic rocks have been identified along the southwestern margin of the NCC or surrounds, suggesting that the source of the 194±3 Ma zircons was the protolith of the greenschist.

5) Late Triassic to Early Jurassic basalts occurred at Rujigou on the northwestern margin of the NCC (Fig. 1(b)) and, as both the study area and Rujigou basalt lie in the western margin of the NCC, it is possible that similar extensional processes occurred in the study area at this time. The Rujigou basalt (36.5 m thick) overlies clastic

Table 2 LA-ICP-MS U–Pb data for zircons from greenschists and the interbedded siltstones within greenschists

Sample	Spot no.	Pb* /ppm	^{232}Th /ppm	^{238}U /ppm	Th/U	Isotopic ratios						Ages/Ma					
						^{207}Pb/^{206}Pb		^{207}Pb/^{235}U		^{206}Pb/^{238}U		^{207}Pb/^{206}Pb		^{207}Pb/^{235}U		^{206}Pb/^{238}U	
						ratios	1s	ratios	1s	ratios	1s	Ages	1s	Ages	1s	Ages	1s
16LP05 (Collected at ⑥ observation spot)	1	32.4	86.59	69.82	1.24	0.1119	0.003	4.803	0.097	0.311	0.004	1830	18	1785	17	1747	21
	3	250.4	64.66	647.74	0.1	0.1236	0.001	5.615	0.04	0.33	0.002	2008	17	1918	6	1837	10
	5	30.2	24.66	71.44	0.35	0.1159	0.002	5.479	0.073	0.343	0.003	1894	12	1897	11	1900	16
	6	13.9	106.72	158.65	0.67	0.0562	0.002	0.529	0.017	0.068	0.001	460	44	431	11	425	6
	7	40.4	298.58	503.76	0.59	0.0551	0.001	0.478	0.009	0.063	0.001	417	24	397	6	393	4
	8	158.9	21.85	316.53	0.07	0.1392	0.002	7.968	0.071	0.415	0.003	2218	7	2227	8	2238	14
	10	164.2	31.69	404.52	0.08	0.1231	0.001	5.944	0.044	0.35	0.002	2001	18	1968	6	1936	10
	11	160.1	35.68	380	0.09	0.1227	0.001	6.133	0.046	0.362	0.002	1996	6	1995	7	1994	11
	12	152	12.69	363.01	0.03	0.1237	0.001	6.221	0.047	0.365	0.002	2010	6	2007	7	2005	11
	15	28.3	316.27	283.31	1.12	0.06	0.001	0.583	0.011	0.071	0.001	602	24	467	7	439	4
	16	108.6	179.66	249.83	0.72	0.1145	0.001	5.166	0.047	0.327	0.002	1872	8	1847	8	1825	12
	17	155.2	33.66	356.57	0.09	0.1216	0.001	6.097	0.051	0.364	0.002	1980	19	1990	7	1999	11
	20	41.5	458.05	383.82	1.19	0.0617	0.003	0.629	0.025	0.074	0.001	662	90	495	15	460	5
	22	17.4	131.52	189.93	0.69	0.0591	0.002	0.589	0.014	0.072	0.001	570	32	470	9	450	5
	24	122.3	24.67	285.36	0.09	0.1248	0.001	6.408	0.051	0.372	0.003	2026	6	2033	7	2041	12
	28	143.3	27.82	370.5	0.08	0.1235	0.001	5.717	0.048	0.336	0.002	2008	20	1934	7	1866	11
	29	216.4	121.64	363.69	0.33	0.16	0.002	10.53	0.082	0.478	0.003	2455	6	2483	7	2517	14
	33	192.2	57.87	435.42	0.13	0.1256	0.001	6.618	0.049	0.382	0.002	2038	6	2062	6	2086	12
	34	34.6	59.81	87.79	0.68	0.1049	0.002	4.408	0.076	0.305	0.004	1713	16	1714	14	1715	17
	35	22.5	92.07	280.15	0.33	0.0554	0.002	0.518	0.017	0.068	0.001	427	80	424	11	423	5
	36	206.2	76.41	524.39	0.15	0.1214	0.001	5.674	0.046	0.339	0.002	1976	19	1927	7	1882	11

(*Continued*)

Sample	Spot no.	Pb* /ppm	^{232}Th /ppm	^{238}U /ppm	Th/U	Isotopic ratios						Ages/Ma					
						^{207}Pb/^{206}Pb		^{207}Pb/^{235}U		^{206}Pb/^{238}U		^{207}Pb/^{206}Pb		^{207}Pb/^{235}U		^{206}Pb/^{238}U	
						ratios	1s	ratios	1s	ratios	1s	Ages	1s	Ages	1s	Ages	1s
14LP03 (Collected at ⑤ observation spot)	1	8.17	79.34	84.52	0.94	0.0571	0.0031	0.5651	0.0285	0.0717	0.0011	496	85	455	19	446	6
	2	125.4	133.87	747.28	0.18	0.0708	0.0016	1.4757	0.02	0.1511	0.0015	951	13	920	8	907	8
	4	86.82	548.29	1273.57	0.43	0.0622	0.0016	0.4923	0.0085	0.0574	0.0006	525	64	381	8	358	4
	5	25.06	43	62.53	0.69	0.1163	0.0034	4.9619	0.1129	0.3092	0.0042	1900	22	1813	19	1737	21
	6	11.7	31.95	30.67	1.04	0.11	0.0039	4.1077	0.1232	0.2707	0.0042	1799	32	1656	24	1544	22
	8	224.32	232.55	411.77	0.56	0.1606	0.0035	9.2603	0.1048	0.418	0.0042	2462	9	2364	10	2251	19
	9	12.19	133.01	134.62	0.99	0.0609	0.0027	0.5615	0.022	0.0669	0.0009	634	61	453	14	417	5
	10	26.05	42.42	64.54	0.66	0.1145	0.0031	4.9062	0.1014	0.3107	0.0039	1872	20	1803	17	1744	19
	11	12.73	179.92	132.62	1.36	0.1182	0.0046	0.9433	0.0309	0.0579	0.0008	656	225	380	31	337	6
	13	29.66	235.37	190.39	1.24	0.0742	0.0023	1.0371	0.0252	0.1014	0.0012	1046	30	722	13	622	7
	15	28.1	234.81	298.24	0.79	0.0581	0.0019	0.584	0.0151	0.0729	0.0008	534	36	467	10	453	5
	16	23.24	309.58	243.32	1.27	0.055	0.0019	0.5082	0.0149	0.067	0.0008	412	44	417	10	418	5
	17	12.67	118.83	139.4	0.85	0.057	0.0025	0.5438	0.0208	0.0691	0.0009	493	61	441	14	431	5
	18	8.4	59.99	80.82	0.74	0.0673	0.0034	0.6943	0.0321	0.0748	0.0012	503	174	467	28	459	7
	19	44.65	727.02	432.77	1.68	0.063	0.0018	0.5776	0.0128	0.0665	0.0007	709	29	463	8	415	4
	20	26.36	328.09	592.02	0.55	0.0755	0.0028	0.3487	0.011	0.0335	0.0004	224	146	207	12	206	3
	21	28.62	196.15	261.53	0.75	0.0674	0.0022	0.7793	0.02	0.0839	0.001	850	34	585	11	519	6
	22	19.75	44	45.86	0.96	0.1124	0.0042	4.8325	0.1603	0.3119	0.0054	1838	35	1791	28	1750	27
	28	37.73	405.57	438.11	0.93	0.0561	0.0017	0.5	0.0122	0.0647	0.0007	456	34	412	8	404	4
	29	37.96	512.81	374.67	1.37	0.0715	0.0021	0.6627	0.0151	0.0672	0.0008	537	134	432	20	412	5
	30	23.02	196.75	249.1	0.79	0.0599	0.002	0.5926	0.0166	0.0718	0.0009	601	40	473	11	447	5
	31	20.9	150.63	227.75	0.66	0.075	0.0025	0.7091	0.0192	0.0686	0.0008	555	116	441	18	419	5
	32	128.77	82.79	334.95	0.25	0.1203	0.0027	5.4246	0.0685	0.3273	0.0034	1960	10	1889	11	1825	17

(*Continued*)

Sample	Spot no.	Pb* /ppm	^{232}Th /ppm	^{238}U /ppm	Th/U	Isotopic ratios						Ages/Ma					
						^{207}Pb/^{206}Pb		^{207}Pb/^{235}U		^{206}Pb/^{238}U		^{207}Pb/^{206}Pb		^{207}Pb/^{235}U		^{206}Pb/^{238}U	
						ratios	1s	ratios	1s	ratios	1s	Ages	1s	Ages	1s	Ages	1s
14LP04 (Collected at ④ observation spot)	1	35.53	199.78	280.24	0.71	0.0801	0.0026	1.1174	0.0286	0.1012	0.0012	1059	87	721	21	617	8
	2	13	202.75	130.53	1.55	0.0592	0.0026	0.5453	0.0212	0.0668	0.0009	575	61	442	14	417	5
	4	44.78	400.66	496.53	0.81	0.0579	0.0016	0.5661	0.0116	0.0709	0.0008	525	26	455	8	442	5
	5	57.09	27.81	179.09	0.16	0.1222	0.0032	4.5711	0.0853	0.2712	0.0033	1859	45	1674	17	1530	17
	6	10.34	98.29	117.24	0.84	0.0601	0.0026	0.5694	0.0222	0.0687	0.0009	608	60	458	14	428	6
	7	69.24	156.11	158.28	0.99	0.1206	0.0029	5.4044	0.0817	0.3249	0.0036	1965	13	1886	13	1814	18
	8	27.4	259.06	294.82	0.88	0.0636	0.002	0.6194	0.0153	0.0706	0.0008	729	33	489	10	440	5
	9	69.12	168.46	158.28	1.06	0.1239	0.0032	5.7232	0.1079	0.3348	0.0042	2014	17	1935	16	1862	20
	10	10.53	108.53	116.18	0.93	0.0585	0.0026	0.5599	0.0228	0.0694	0.001	550	64	451	15	432	6
	11	21.41	183.74	242.59	0.76	0.0569	0.002	0.551	0.0158	0.0702	0.0008	489	42	446	10	437	5
	12	19.11	158.12	220.33	0.72	0.056	0.002	0.54	0.0167	0.0699	0.0009	454	47	438	11	435	5
	13	138.91	269.57	163.69	1.65	0.2281	0.0051	18.4964	0.2458	0.5878	0.0067	3039	10	3016	13	2981	27
	14	11.81	91.98	142.44	0.65	0.0569	0.0024	0.5274	0.0199	0.0672	0.0009	488	60	430	13	419	5
	15	11.33	22.16	29.45	0.75	0.1079	0.0043	4.3776	0.158	0.2941	0.0053	1675	105	1662	43	1651	28
	18	38.88	274.83	291.65	0.94	0.0715	0.0032	0.5879	0.0238	0.0596	0.0009	511	173	387	24	367	6
	19	12.11	194.73	240.07	0.81	0.0813	0.0032	0.4076	0.0139	0.0364	0.0005	337	171	232	15	222	3
	20	99.05	244.12	212.18	1.15	0.1213	0.0028	5.5012	0.0784	0.3289	0.0036	1975	12	1901	12	1833	17
	21	55.48	211.45	332.88	0.64	0.0691	0.0018	1.2796	0.0231	0.1342	0.0015	902	20	837	10	812	8
	22	21.48	469.62	451.89	1.04	0.0495	0.0019	0.2465	0.008	0.0361	0.0004	173	54	224	7	229	3
	23	20.39	381.03	440.83	0.86	0.0493	0.0019	0.2447	0.0079	0.036	0.0004	163	53	222	6	228	3
	24	15.3	146.76	175.59	0.84	0.0542	0.0022	0.5087	0.0178	0.0681	0.0009	379	55	418	12	425	5
	25	16.12	101.39	194.07	0.52	0.0565	0.0021	0.5425	0.0174	0.0697	0.0009	471	49	440	11	434	5
	26	70.1	559.16	849.72	0.66	0.0561	0.0014	0.5165	0.0091	0.0668	0.0007	455	21	423	6	417	4
	27	43.29	87.78	591.28	0.15	0.0568	0.0015	0.5299	0.0105	0.0677	0.0007	482	25	432	7	422	4
	29	43.95	439.95	489.38	0.9	0.0565	0.0016	0.5314	0.0115	0.0682	0.0008	472	29	433	8	425	5
	30	27	265.3	302.29	0.88	0.059	0.0019	0.5526	0.0143	0.068	0.0008	565	36	447	9	424	5
	33	26.03	12.71	68.24	0.19	0.1173	0.0032	5.4684	0.114	0.3382	0.0045	1915	20	1896	18	1878	22
	34	27.77	323.26	284.38	1.14	0.0566	0.0019	0.5575	0.0155	0.0714	0.0009	477	41	450	10	445	5
	36	106.83	102.37	374.38	0.27	0.0952	0.0022	3.2884	0.0462	0.2505	0.0027	1471	39	1450	13	1436	14
	37	23.73	246.02	252.5	0.97	0.0548	0.0019	0.5275	0.0156	0.0699	0.0009	402	44	430	10	435	5
	38	25.07	359.3	243.87	1.47	0.0561	0.0019	0.5328	0.0155	0.0689	0.0008	455	43	434	10	430	5
	39	11.29	117.82	263.15	0.45	0.0903	0.0042	0.4013	0.0169	0.0322	0.0005	107	185	187	14	194	3
	40	52.6	17.97	130.48	0.14	0.121	0.0029	5.9466	0.0978	0.3565	0.0042	1971	14	1968	14	1966	20

Note: Pb* represents radiogenic lead in this table.

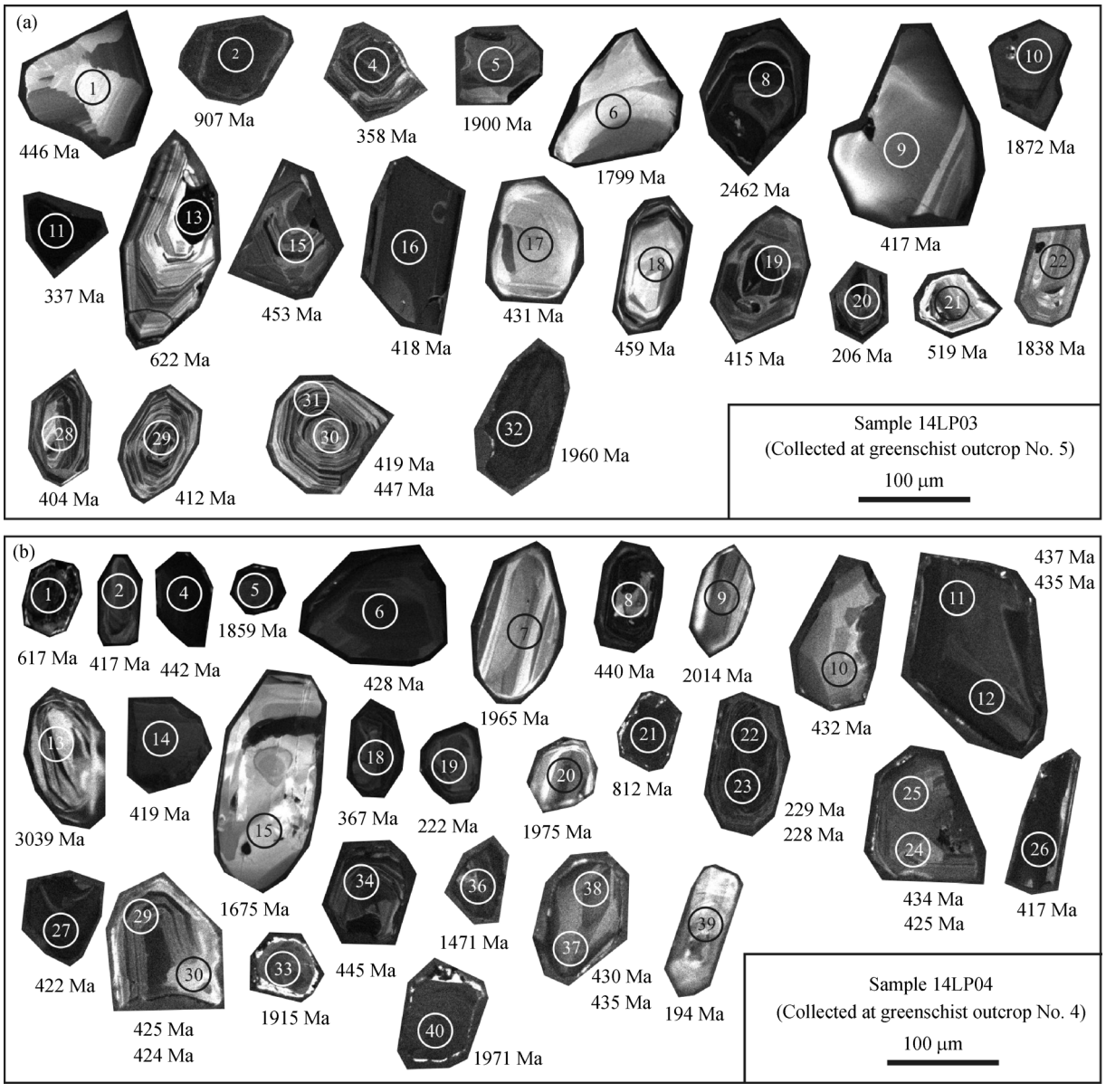

Fig. 11 Cathodoluminescence (CL) images of zircons from the siltstones interbedded with the greenschists. Circles indicate analysis sites, and figures within the circles are analysis numbers; the ages are given below the corresponding zircons.

rocks of the Upper Triassic Yanchang Formation and is overlain by Middle Jurassic sedimentary rocks. It has been extensively altered, with alteration decreasing in intensity towards the central parts of the basalt, and containing abundant chlorite (Yang et al., 2010). Although several studies have obtained a range of ages (229±15 Ma, Bureau of Geology and Mineral Resources of Ningxia Hui Autonomous Region, 1990; 193–229 Ma, Wang et al., 2005) for the Rujigou basalt, its contacts with adjacent strata indicate an age of Late Triassic to Early Jurassic. The continental tholeiitic Rujigou basalt (Yang et al., 2010) was formed in a continental rift environment (Wang et al., 2005), revealing that rifting occurred along the northwestern margin of the NCC during the Late Triassic and Early Jurassic. The ages of the Rujigou basalt are similar to the youngest zircon ages obtained in this study; therefore, we propose that the basalt and the protolith of the greenschists in the study area are coeval. This hypothesis is supported by the occurrence of the Upper Triassic Yanchang Formation in both areas (Fig. 1(b)). The protolith was metamorphosed under greenschist-facies conditions by extensive faulting compression and burial related to movement along the Liupanshan Fault system during the Late Jurassic and Early Cretaceous, reflected by the thick deposits of coeval conglomerates. However, the Rujigou basalt was only weakly metamorphosed as it lies distant from the Liupanshan Fault system. In addition, tuff intervals of Upper Triassic Yanchang Formation are

laterally widespread in the Ordos basin, suggesting the coeval volcanic activity around the Ordos block (Qiu et al., 2014).

4.2 Reassignment of the greenschists

The youngest zircon ages of the siltstones interbedded with the greenschists indicate that the formation age of the protolith of the greenschists cannot be earlier than 193–206 Ma; therefore, the greenschists should not be considered part of the Paleoproterozoic stratigraphic unit. In addition, detrital zircons from blastolithic sandstones of the low-grade metasedimentary rocks of the former Xiong'er Group yield concordant U–Pb ages of 1091–2854 Ma (to be discussed in a forthcoming article). Consequently, the sedimentation could not have pre-dated 1091 Ma and the Xiong'er Group may not have developed on the southwestern margin of the NCC. This would account for the differences in lithological associations and ages of deformation between the Xiong'er Group on the southwestern margin of the NCC, and the group located in the Xiong'ershan, Xiaoshan, and Xiaoqinling mountains (Fig. 1(b)).

4.3 Provenance of siltstones interbedded with the greenschists

The ages (412–480 Ma) of siltstones interbedded with the greenschists (Fig. 12) correspond to the ages of several basic and acidic magmatic rocks (413–462 Ma) (Zhang et al., 2006; Chen et al., 2007; He et al., 2007; Pei et al., 2007a, b; Wei et al., 2012; Wang, 2013; Wei, 2013) in the Longshan area, west of the present study area (Table 4). Therefore, it is possible that the magmatic suites in the Longshan area were the source of the siltstones.

The age peak of 2000 Ma (Fig. 12) is similar to that of the NCC basement and to granite–gneisses of the Longshan Complex (1.90 Ga–1.95 Ga; He et al., 2005).

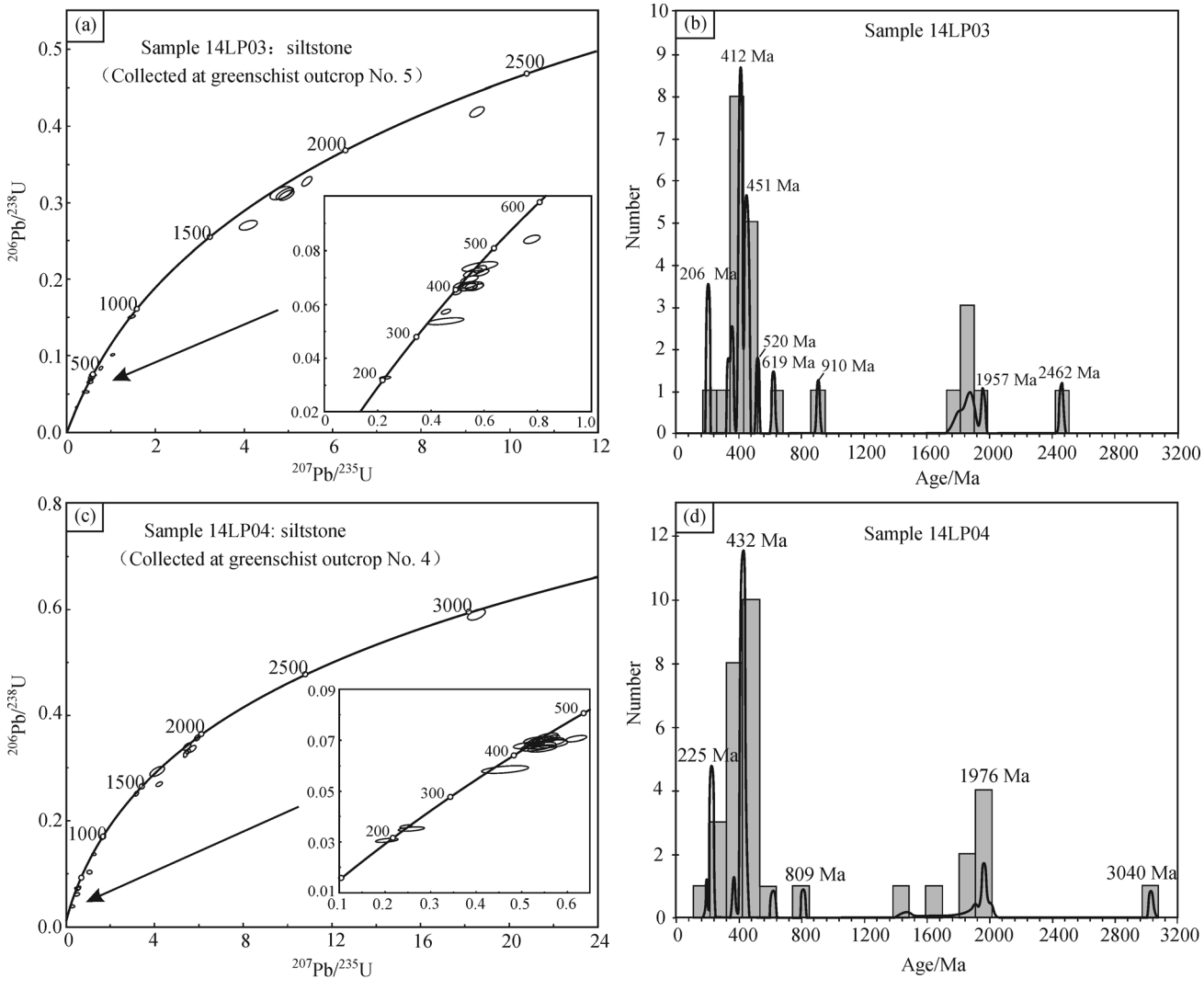

Fig. 12 Concordia diagrams for the siltstones interlayered with the greenschists. Interpreted ages are $^{206}Pb/^{238}U$ for zircons with ages of < 1.0 Ga and $^{207}Pb/^{206}Pb$ for zircons with ages of > 1.0 Ga.

Table 3 Magmatic rocks of Late Triassic in the western Qinling orogen and Longshan area

Position	Rock type	Method	Age/Ma	References
Shangdan suture in the Qinling orogenic belt	Lamprophyre	$^{40}Ar/^{39}Ar$	219±2	Wang et al., 2007
Western Qinling orogenic belt	Rhyolite	Zircon U-Pb LA-ICP-MS	211±6	Xu et al., 2007
Western Qinling orogenic belt	Medium-fine-grained two mica granite	Zircon U-Pb LA-ICP-MS	213 + 2~214 + 1	Wang et al, 2011
Longshan	Monzogranite	Zircon U-Pb SHRIMP	229±7	Zhang et al., 2006
Western Qinling orogenic belt	Monzogranite	Zircon U-Pb LA-ICP-MS	213±3	Qin et al, 2009
Qinling	Granitoids, diorite	Zircon U-Pb SHRIMP	227~218	Jiang et al., 2010
Western Qinling orogenic belt	Rhyolite	Zircon U-Pb LA-ICP-MS	214.6±8	Qiu, 2011
Western Qinling orogenic belt	quartz monzodiorite	Zircon U-Pb LA-ICP-MS	214.5±1.6	Li et al., 2013
Western Qinling orogenic belt	Quartz orthophyre	Zircon U-Pb LA-ICP-MS	209.3±5.8	Ding et al., 2015

Table 4 Magmatic rocks with formation ages of 413– 452 Ma in the Longshan area

Rock type	Method	Age/Ma	References
Metamorphic intermediate- acidic volcanic rocks	Zircon U-Pb LA-ICP-MS	461.2±3.1	Wei, 2013
Metamorphic intermediate- acidic volcanic rocks	Zircon U-Pb LA-ICP-MS	462.4±3.4	Wei, 2013
Basalt	Zircon U-Pb LA-ICP-MS	443.4±1.7	He et al., 2007
Granodiorite	Zircon U-Pb LA-ICP-MS	457.0±3.2	Wei, 2013
Granodiorite	Zircon U-Pb LA-ICP-MS	440.5±4.4	Wei et al., 2012
Quartz diorite	Zircon U-Pb LA-ICP-MS	454.7±1.7	Chen et al., 2007
Diorite	Zircon U-Pb SHRIMP	441±10	Zhang et al., 2006
Diorite	Zircon U-Pb LA-ICP-MS	440.2±0.92	Pei et al., 2007a
Monzogranite	Zircon U-Pb SHRIMP	434±10	Zhang et al., 2006
Medium-coarse grained gabbro	Zircon U-Pb LA-ICP-MS	434.6±1.5	Pei et al., 2007b
Medium-coarse grained porphyroid syenogranite	Zircon U-Pb LA-ICP-MS	413.8±2.1	Wang, 2013
Syenogranite	Zircon U-Pb LA-ICP-MS	423.8±2.8	Wang, 2013
Syenogranite	Zircon U-Pb LA-ICP-MS	438.1±2.6	Wang, 2013

Therefore, this age likely represents the age of amalgamation of the Columbia Supercontinent.

4.4 Late Triassic to Early Jurassic tectonic environment along the southwestern margin of the North China Craton

The Late Triassic to Early Jurassic continental tholeiite protolith of greenschists in the Xiong'er Group indicates that the tectonic regime at the time was dominated by extension. This tectonic setting was also responsible for the distribution of Late Triassic sediments in the area (Zhao et al., 2006; Deng et al., 2008). The Late Triassic mafic or alkaline rocks and intrusions occurred on the northern and southern margins of the North China Craton and Xingmeng Orogenuc belt, implying that intensified extension occurred across the entire region of North China (Liu et al., 2015). Han et al. (2014) proposed that Late Triassic sedimentation occurred in a region of steep topography caused by NE-trending compression in the Qinling Orogen (Feng et al., 2009), and that the source of sediments was close to their sites of deposition. Liu et al. (2013) proposed that the Late Triassic continuous subsidence and deposition within the Ordos basin were predominantly related to the thrust load of the East Qilian–Qinling belt and inferred mantle flow effects associated with paleotethys plate subduction. The present results show that even though Late Triassic regional compression was unlikely to have occurred along the southwestern margin of the NCC, regional extension did occur.

While widespread sedimentation occurred during the Early Jurassic, the occurrence of Lower Jurassic strata in the area was limited. This could reflect the deep burial of Lower Jurassic strata, or the extensive denudation of these rocks between the Late Jurassic and Early Cretaceous, which may have acted as the source of the widespread Upper Jurassic Fenfanghe Formation and Lower Cretaceous Liupanshan Group conglomerates along the southwestern margin of the NCC. The denudation from the Late

Jurassic to Early Cretaceous not only explains the absence of Lower Jurassic strata, but also fragmented the Upper Triassic Yanchang Formation, which consists of fine-grained clastic rocks scattered throughout the study and adjacent areas.

The ages of detrital zircons in siltstones (400 Ma) correspond with those obtained from the magmatic rocks from the western Qinling Orogen; therefore, the tectonic environment in which the study area developed may have formed as a result of post-collisional extension associated with orogenesis, which continued throughout the Late Triassic and Early Jurassic. Huang et al. (2013) proposed that 229 Ma rhyolites, trachytes, and dacites in the western Qinling Orogen formed under regional conditions of crustal thickening and compression, and local shearing-related extension; however, numerous Late Triassic magmatic rocks (Table 3) provide evidence of regional extension.

A second mechanism that could account for Late Triassic to Early Jurassic extension is continental rifting resulting from geodynamic processes in the lower lithosphere. The greenschists in the study area have geochemical characteristics of continental tholeiitic basalt. We obtained ε_{Nd} (t = 200 Ma) = 3.38, reflecting limited crustal contamination. The average $^{143}Nd/^{144}Nd$ value for the greenschist is 0.512835, which is near-chondritic, and the average ε_{Nd} (t = 1672 Ma) is 3.78, suggesting that the protolith of the greenschists was derived from a depleted mantle source (Zhou et al., 1994).

Figure 13 shows that the greenschist samples fall between N-MORB, E-MORB, and intraplate tholeiites in tectonic discrimination diagrams, suggesting that their protolith was contaminated by crustal material. Due to the absence of an oceanic environment in the study area during the Late Triassic to Early Jurassic, we propose that continental rifting was the dominant process responsible for the formation of the protolith of the greenschists. However, post-collisional extension in the western Qinling Orogen may have contributed to regional extension along the southwestern margin of the NCC.

The 193–229 Ma Rujigou basalt may be considered additional evidence for continental rifting in the study area. This basalt occurs between the Ordos Block in the east and the Alanshan Block in the west. Post-collisional extension, similar to that in the western Qinling Orogen, did not occur in this region at that time; therefore, the Rujigou basalt likely formed as a result of geodynamic processes in the lower lithosphere. Granodiorites (223±26 Ma) occur at the southern margin of the Helanshan Mountains (Bai and Lu, 2009), near the Rujigou basalt. Together, these units may constitute a bimodal magmatic suite. Similarities in age, geochemistry, and location indicate that the Rujigou basalt and the protolith of the greenschists in the Xiong'er Group were generated by similar tectonic processes, particularly continental rifting (Wang et al., 2005; Yang et al., 2010).

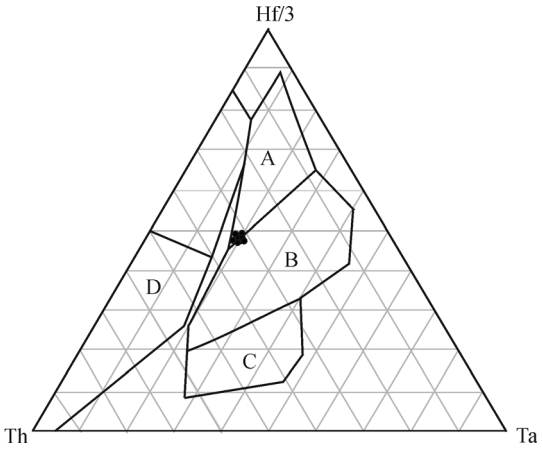

Fig. 13 Discrimination diagram for the greenschists (after Wood, 1980). A = N-MORB; B = E-MORB and intraplate tholeiite; C = intraplate alkaline basalt; D = volcanic arc basalt.

5 Conclusions

1) Detrital zircons from two siltstone interlayers within greenschists are proposed to be part of the Paleoproterozoic Xiong'er Group at the southwestern margin of the NCC yield concordant U–Pb ages ranging from 3039 to 194 Ma. Based on these ages and regional geological data, we propose that the protolith of the greenschists were formed between the Late Triassic and Early Jurassic (206–194 Ma); therefore, the greenschists should be reclassified and removed from the former Xiong'er Group.

2) The protolith of the greenschists was continental tholeiitic basalt that formed in a continental rift environment. This protolith was metamorphosed under conditions of the greenschist facies, likely related to extensive faulting in the Liupanshan Fault system during the Jurassic.

3) Late Triassic, post-collisional extension of the western Qinling Orogen may have contributed to regional extension along the southwestern margin of the NCC.

4) Late Triassic to Early Jurassic extension took place at the southwestern margin of the NCC, rather than subsidence of a foreland basin under regional compression.

Acknowledgements Financial support for this study was jointly provided by the National Natural Science Foundation of China (Grant No. 41421002) and MOST Special Fund from the State Key Laboratory of Continental Dynamics, Northwest University.

References

Bai S M, Lu C G (2009). The characteristics and age of south section of Helanshan Dazhangchang granodiorite. NingXia Enginering Technology, 8: 282–286 (in Chinese)

Baoji Geological Map (1966). Shaanxi Institute of Geological Survey

Baojishi Geological Map (2003). Shaanxi Institute of Geological Survey

Boynton W W (1984). Cosmochemistry of the rare earth elements: meteorite studies. In: Henderson P, ed. Rare Earth Element Geochemistry: Developments in Geochemistry 2. Amsterdam: Elsevier, 63–114

Bureau of Geology and Mineral Resources of Ningxia Hui Autonomous Region (1990). Regional geology of Ningxia Hui Autonomous Region. Beijing: Geological Publishing House, p. 331 (in Chinese)

Bureau of Geology and Mineral Resources of Shaanxi Province (1989). Regional Geology of Shaanxi Province. Beijing: Geological Publishing House, p. 243 (in Chinese)

Chen J L, Li H B, Wang H L, He S P, Zeng Z X, Xu X Y, Li X M (2007). LA-ICPMS Zircon U-Pb dating of a quartz diorite pluton from Wangjiacha, the junction area between the Qinling and Qilian orogenic belts and its tectonic significance. Journal of Jilin University (Earth Science Edition), 37: 423–431

Cui M L, Zhang B L, Zhang L C (2011). U-Pb dating of baddeleyite and zircon from the Shizhaigou diorite in the southern margin of North China Craton: constrains on the timing and tectonic setting of the Paleoproterozoic Xiong'er Group. Gondwana Res, 20(1): 184–193

Deng X H, Chen Y J, Santosh M, Yao J M (2013). Genesis of the 1.76 Ga Zhaiwa Mo-Cu and its link with the Xiong'er volcanics in the North China Craton: implications for accretionary growth along the margin of the Columbia supercontinent. Precambrian Res, 227: 337–348

Deng X Q, Lin F X, Liu X Y, Pang J L, Lu J W, Li S X, Liu X (2008). Discussion on relationship between sedimentary evolution of the Triassic Yanchang Formation and the Early Indosinian Movement in Ordos Basin. Journal of Paleogeography, 102: 159–166 (in Chinese)

Ding S Z, Luo J H, Cheng J X, Han K, Wang S D, You J (2015). Geochemistry and chronology of quartz orthophyre in Boyang of the western Qinling orogenic belt, and their geological significance. Earth Sci Front, 22: 247–254 (in Chinese)

Feng S B, Yuan X Q, He J, Wang C Y, Han P, Li W C, Li T Y (2009). Sedimentary tectonic setting of Upper Triassic Yaoshan Formation of Liupanshan area of western Ordos basin. Low Permeability Oil & Gas Fields, 3: 1–5 (in Chinese)

Frey F A, Green D H, Roy S D (1978). Integrated models of basalt petrogenesis: a study of quartze tholeiites to olivine molarities from south eastern Australia utilizing geochemical and experimental petrological data. J Petrol, 19(3): 463–513

Günther D, Hattendorf B (2005). Solid sample analysis using laser ablation inductively coupled plasma mass spectrometry: TrAC. Trends Analyt Chem, 24(3): 255–265

Han P, Feng S B, Li X M, Wang K L, Yuan X Q, He J, Hu A P (2014). Geological evidence of "the archaic uplift" of Late Triassic in western margin of Ordos basin and identification of original boundary in the west of basin. Journal of Oil and Gas Technology, 36: 1–5 (in Chinese)

He S P, Wang H L, Xu X Y, Zhang H F, Ren G M (2007). A LA-ICP-MS U-Pb chronological study of zircons from Hongtubu basic volcanic rocks and its geological significance in the east segment of north Qilian orogenic belt. Advances in Earth Science, 22: 143–151 (in Chinese)

He Y H, Sun Y, Chen L, Li H P, Yuan H L, Liu X M (2005). Zircon U-Pb chronology of Longshan complex by LA-ICP-MS and its geological significance. Acta Petrologica Sinica, 21: 125–134 (in Chinese)

He Y H, Zhao G C, Sun M, Xia X P (2009). SHRIMP and LA-ICP-MS zircon geochronology of the Xiong'er volcanic rocks: implications for the Paleo-Mesoproterozoic evolution of the southern margin of the North China Craton. Precambrian Res, 168(3–4): 213–222

Hou G T, Li J H, Liu Y L, Qian Xi L (2008). The late Paleoproterozoic extension event: aulacogens and dyke swarms in the North China Craton. Prog Nat Sci, 16(2): 201–208

Huang F X, Mo X X, Yu X H, Li X W, Ding Y, Wei P, He W Y (2013). Zircon U-Pb chronology, geochemistry of the Late Triassic acid volcanic rocks in Tanchang area, West Qinling and their geological significance. Acta Petrologica Sinica, 29: 3968–3980 (in Chinese)

Irvine T N, Baragar W R A (1971). A guide to the chemical classification of the common volcanic rocks. Can J Earth Sci, 8: 523–548

Jiang Y H, Jin G D, Liao S Y, Zhou Q, Zhao P (2010). Geochemical and Sr-Nd-Hf isotopic constraints on the origin of Late Triassic granitoids from the Qinling orogen, central China: implications for a continental arc to continent-continent collision. Lithos, 117(1–4): 183–197

Le Bas M J, Le Maitre R W, Streckeisen A, Streckeisen A, Zanettin B (1986). A chemical classification of volcanic rocks based on the total alkali-sillica diagram. J Petrol, 27(3): 745–750

Li Z C, Pei X Z, Li R B, Pei L, Hu B, Liu C J, Chen G C, Chen Y X (2013). LA-ICP-MS zircon U-Pb dating, geochemistry of the Mishuling intrusion in western Qinling and their tectonic significance. Acta Petrologica Sinica, 29: 2617–2634 (in Chinese)

Liu S F, Su S, Zhang G W (2013). Early Mesozoic basin development in North China: indications of cratonic deformation. J Asian Earth Sci, 62(30): 221–236

Liu Y Q, Kuang H W, Peng N, Xu H, Zhang P, Wang N S, An W, Wang Y, Liu M, Hu X F (2015). Mesozoic basins and associated paleogeographic evolution in North China. Journal of Palaeogeography, 4(2): 189–202

Lu S N, Yang C L, Li H K, Li H M (2002). A group of rifting events in the terminal Paleoproterozoic in the North China Craton. Gondwana Res, 5(1): 123–131

Ludwig K R (2001). Users Manual for Isoplot/Ex Rev. 2.49. Berkeley Geochronology Centre Special Publication (No. 1a), 1–56

Pearce J A (1982). Trace element characteristics of lave from destructive plate boundaries. Chichester: Wiley, 525–548

Pei X Z, Ding S P, Zhang G W, Liu H B, Li Z C, Li G Y, Liu Z Q, Meng Y (2007b). The LA-ICP-MS zircons U-Pb ages and geochemistry of the Baihua basic igneous complexes in Tianshui area of West Qinling. Sci China Earth Sci, 50(S2): 264–276

Pei X Z, Sun R Q, Ding S P, Liu H B, Li Z C, Liu Z Q, Meng Y (2007a). LA-ICP-MS zircon U-Pb dating of the Yanjiadian diorite in the eastern Qilian Mountains and its geological significance. Geology in China, 34: 8–16 (in Chinese)

Peng P, Wang X P, Lai Y, Wang C, Windley B F (2015). Large-scale liquid immiscibility and fractional crystallixation in the 1780 Ma Taihang dyke swarm: implications for genesis of the bimodal Xiong'er volcanic province. Lithos, 236–237: 106–122

Peng P, Zhai M G, Richard E (2008). A 1.78 Ga large igneous province in the North China Craton: the Xiong'er Volcanic Province and the North China dyke swarm. Lithos, 101(3–4): 260–280

Qin J F, Lai S C, Grapes R, Diwu C R, Ju Y J, Li Y F (2009). Geochemical evidence for origin of magma mixing for the Triassic monzonitic granite and its enclaves at Mishuling in the Qinling orogen (central China). Lithos, 112(3–4): 259–276

Qiu X W (2011). Characteristic and dynamic settings of Yanchang period hydrocarbon-rich depression in Ordos basin, China. Dissertation for PhD degree. Xi'an: Northwest University, 1–80 (in Chinese)

Qiu X W, Liu C Y, Mao G Z, Deng Y, Wang F F, Wang J Q (2014). Late Triassic tuff intervals in the Ordos basin, Central China: their depositional, petrographic, geochemical characteristics and regional implications. J Asian Earth Sci, 80(5): 148–160

Sun S S, McDonough W F (1989). Chemical and isotope systematics of ocean baslt: implications for mantle composition and processes. In: Saunders A D, Norry M J, eds. Magmatism in the Ocean Basins. Geological Society Special Publication, 42: 313–345

Wang F, Liu C Y, Yang X K, Su C Q (2005). Geologic geochemical features of basalt in Ruqi clough of Helan Mountain and its structural environmental significance. Petroleum Geology & Oilfield Development in Daqing, 24: 25–27 (in Chinese)

Wang T G, Ni P, Sun W D, Zhao K D, Wang X D (2011). Zircon U-Pb ages of granites at Changba and Huangzhuguan in western Qinling and implications for source nature. Science Bulletin, 56(7): 659–669

Wang X L, Jiang S Y, Dai B Z (2010). Melting of enriched Archean subcontinental lithospheric mantle: evidence from the ca. 1760 Ma volcanic rocks of the Xiong'er Group, southern margin of the North China Craton. Precambrian Res, 182(3): 204–216

Wang X X, Wang T, Jahn B M, Hu N G, Chen W (2007). Tectonic significance of Late Triassic post-collisional lamprophyre dykes from the Qinling Mountains (China). Geol Mag, 114: 837–848

Wang Y C (2013). Geological characteristics and tectonic significance of Caledonian collision-post collision type granite at the conjunction of Qinling and Qilian. Dissertation for Master degree. Xi'an: Chang'an University, 1–68 (in Chinese)

Wei F H (2013). Composition, structural characteristics and geological evolution of north Qilian orogen (the eastern) in Early Paleozoic. Dissertation for Master degree. Xi'an: Chang'an University, 1–65 (in Chinese)

Wei F H, Pei X Z, Li R B, Li Z C, Pei L, Gao J M, Wang Y C, Liu C J, Wu S K, Chen Y X (2012). LA-ICP-MS zircon U-Pb dating of Early Paleozoic Huangmenchuan granodiorite in Tianshui area of Gansu Province and its tectonic significance. Geological Bulletin of China, 31: 1496–1509 (in Chinese)

Wiedenbeck M, Allé P, Corfu F, Griffin W L, Meier M, Oberli F, Vonquadt A, Roddick J C, Speigel W (1995). 3 natural zircon standards for U-Th-Pb, Lu-Hf, traceelement and REE analyses. Geostand Newsl, 19(1): 1–23

Wiedenbeck M, Hanchar J M, Peck W H, Sylvester P, Valley J, Whitehouse M, Kron Z A, Morishita Y, Nasdala L, Fiebig J, Franchi I, Girard J P, Greenwood R C, Hinton R, Kita N, Mason P R D, Norman M, Ogasawara M, Piccoli P M, Rhede D, Satoh H, Schulz-Dobrick B, Skår O, Spicuzza M J, Terada K, Tindle A, Togashi S, Vennemann T, Xie Q, Zheng Y F (2004). Further characterisation of the 91500 zircon crystal. Geostand Geoanal Res, 28(1): 9–39

Wood D A (1980). The application of a Th–Hf–Ta diagram to problems of tectono-magmatic classification and to establishing the nature of crustal contamination of basaltic lavas of the British Tertiary Volcanic Province. Earth Planet Sci Lett, 50(1): 11–30

Xu X Y, Wang H L, Chen J L, Su X H, Wu P, Gao T (2007). Zircon U-Pb age, element geochemistry of Mesozoic acid volcanic rocks at Yindaoshi area in western Qinling. Acta Petrologica Sinica, 23: 2845–2856 (in Chinese)

Yang H, Fu J H, Ouyang Z J, Sun L Y, Ma Z R (2010). U-Pb Zircon Dating of the Daling-Gugutai Basalt in Rujigou on the Western Margin of Ordos Basin. Acta Geoscientica Sinica, 31: 229–236 (in Chinese)

Yu X H, Mo X X, Zhao Z D, He W Y, Li Y (2011). Cenozoic bimodal volcanic rocks of the West Qinling: implication for the genesis and nature of the rifting of north-south tectonic belt. Acta Petrologica Sinica, 27: 2195–2202 (in Chinese)

Zhai M G, Hu B, Zhao T P, Peng P, Meng Q R (2015). Late Paleoproterozoic-Neoproterozoic multi-rifting events in the North China Craton and their geological significance: a study advance and review. Tectonophysics, 662: 153–166

Zhang H F, Zhang B R, Harris H, Zhang L, Chen Y L, Chen N S, Zhao Z D (2006). U-Pb zircon SHRIMP ages, geochemical and Sr–Nd–Pb isotopic compositions of intrusive rocks from the Longshan–Tianshui area in the southeast corner of the Qilian orogenic belt, China: constraints on petrogenesis and tectonic affinity. J Asian Earth Sci, 27 (6): 751–764

Zhang Z, Li S Z, Cao H H, Somerville I D, Zhao S J, Yu S (2015). Origin of the North Qinling Microcontinent and Proterozoic geotectonic evolution of the Kuanping Ocean, Central China. Precambrian Res, 266: 179–193

Zhao G C, He Y H, Sun M (2009). The Xiong'er volcanic belt at the southern margin of the North China Craton: petrographic and geochemical evidence for its outboard position in the Paleo-Mesoproterozoic Columbia Supercontinent. Gondwana Res, 16(2): 170–181

Zhao T P, Xu Y H, Zhai M G (2007). Origin and tectonic setting of the Proterozoic Xiong'er Group volcanic rocks in the southern part of the North China Craton; Facts and controversies. Geological Journal of China Universities, 13(2): 191–206

Zhao T P, Zhai M G, Xia B, Li H M, Zhang Y X, Wan Y S (2004). Zircon U-Pb SHRIMP dating for the volcanic rocks of the Xiong'er Group: constraints on the initial formation age of the cover of the North China Craton. Science Bulletin, 49(23): 2495–2502

Zhao T P, Zhou M F, Zhai M G, Xia B (2002). Palaeoproterozoic rift-related volcanism of the Xiong'er Group in the North China Craton: implications for the break-up of Columbia. Int Geol Rev, 44(4): 336–351

Zhao W Z, Wang X M, Guo Y R, Liu H Q, Bai Y L (2006). Restoration and tectonic reworking of the Late Triassic basin in western Ordos Basin. Petroleum Exploration and Development, 33: 6–13 (in Chinese)

Zhou D W, Zhao C Y, Li Y D, Jian W C, Ye J, Chen G (1994). Geological Features of Southwest Margin of Ordos Basin and Its Relationships With Qinling Orogenic Belt. Beijing: Geological Publishing House, 98–110 (in Chinese)